Director Response of Liquid Crystals in Spatially Varying Magnetic Fields with Antagonistic Anchoring Conditions

*Zhe Liu‡[1], Yvonne Zagzag‡[2], Randall D. Kamien[2], Chinedum O. Osuji[1]**

[1]Department of Chemical and Biomolecular Engineering, University of Pennsylvania, Philadelphia, PA 19104, USA.

[2]Department of Physics and Astronomy, University of Pennsylvania, Philadelphia, PA 19104, USA.

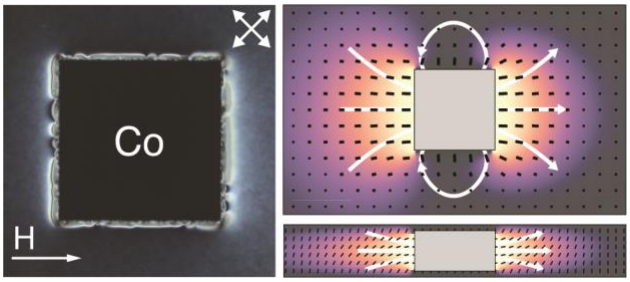

Table of Contents Image

ABSTRACT

In the presence of a magnetic field, an LC director can be distorted from a ground state set by a combination of LC elasticity and surface anchoring at any relevant interfaces. Uniform magnetic fields are often used to produce simple LC distortions on demand, but producing more spatially complex distortions is practically challenging. We develop a strategy for the spatially resolved control of the LC director by leveraging field patterns induced by ferromagnetic materials. Patterned magnetic fields are generated from high permeability ferromagnetic microstructures embedded into nematic liquid crystals (NLCs) to manipulate the LC director's orientation. Each ferromagnetic microstructure produces a unique spatially varying magnetic field. In turn, tuning magnetic field strength in competition with NLC elasticity can pattern a range of spatially complex director configurations. Simulations relate the spatial variation induced in a magnetic field by a ferromagnetic geometry and the resultant director. Our predictive models can inform the inverse design of ferromagnetic microstructures to generate bespoke director patterns. We also link changes in the magnetic field to the migration of elastically driven periodic extinctions in birefringence near the edges of ferromagnetic structures.

KEYWORDS

liquid crystals; magnetic field alignment; spatial materials programming; magnetic field sensing; surface anchoring

INTRODUCTION

The properties of liquid crystal (LC) materials can be controlled by manipulating the orientational order of their constituents. If these properties are controlled spatially, opportunities arise to create new non-trivial types of materials.[1, 2] The anisotropic susceptibility of LCs to external electric and magnetic fields enables relatively facile control over their orientational order. Therefore, it is conceivable that a combination of spatially varying fields can be used to program any anisotropic properties associated with the LC mesophase—elasticity, permittivity, and more.

The ground state of an LC in the absence of external fields is determined by its anchoring at relevant solid boundaries. Within an LC, the director will tend towards a free-energy minimizing configuration that satisfies constraints (e.g., as might be imposed by surfaces); deviations from the energy-minimizing configuration or violations of the constraints incur energetic penalties. A large body of literature documents efforts to control the LC director. Micropatterned silicon treated to apply preferential orientation can pattern the LC director and defect structure.[3-5] Voxels within liquid crystalline elastomers can be programmed via photoalignment and surface chemistry to actuate stimuli-responsive shape transformations that can withstand loads.[6-8] Metamaterials from elastomer composites can be printed with programmed domains of varying magnetic polarity.[9]

It is well known that the ground state of an LC can be modified by introducing an electric or magnetic field.[10] Electric fields, for example, are frequently used to reorient LCs away from a ground state in display applications. By contrast, magnetic fields are less frequently used because the low magnetic susceptibility anisotropy of LCs typically necessitates prohibitively large field strengths.[11] However, magnetic field directed alignment of both small[12] and macromolecular liquid crystals[13-15] and nanocomposites[16, 17] has been demonstrated. Embedding high-permeability magnetic materials into an LC provides a strategy for creating magnetic fields with spatially

varying intensities and local hotspots strong enough to generate a change in the director. This scheme is dependent on the continuity of field lines, which must have a higher density in regions with high permeability. In the presence of a background magnetic field, the convolution of the concentrated field lines around a ferromagnet and the shape of the magnetic material determine the resulting spatial field variation. We use such spatially nonuniform magnetic fields to locally deflect LCs away from their ground state by balancing magnetic susceptibility, elasticity, and proximity of anchoring boundaries.[18, 19] In tandem, at a fixed temperature, surface chemistry dictates the anchoring conditions ruling the distance from a surface over which an elastic-magnetic distortion can propagate into the system.

Here, we demonstrate that the director of a nematic LC can be spatially controlled through tailored spatial magnetic field variations induced by micro-structured high permeability materials. We study small molecule LCs (5CB) in the nematic phase confined in a homeotropic cell as they undergo a bend-type Fréedericksz transition. We model the spatial concentration of magnetic fields near ferromagnetic interfaces using electromagnetic theory and finite element simulations (FEM). We then simulate the LC director response using numerical relaxation of the Landau-de Gennes (LdG) free energy. Polarized optical microscopy (POM) is used to observe the LC director and reveals spatially modified field patterns encoded into the birefringence of the LC. We observe a spatially varying period for birefringence extinction associated with the decay of the magnetic field away from the microstructure and the associated continuous variation of the director, and we account for the optical properties of the system.

EXPERIMENTAL AND SIMULATION METHODS

Ferromagnetic Inclusions in NLC Cells

The NLC cell comprises two glass slides treated with dodecyltrimethoxysilane, a common silane coupling agent, to achieve homeotropic anchoring on their surfaces.[20] 50.8 μm thick cobalt foils were purchased from Alfa Aesar and sent to Braneva Precision where they were cut using Electrical Discharge Machining (EDM) to match the geometries used here. The desired cobalt structure was then sandwiched between two glass slides bonded using optical adhesives. Silica particles with an average size of 60 μm were mixed into the optical adhesives to define the thickness of the cell. The NLC, specifically 4-cyano-4'-pentylbiphenyl (5CB), was added into the cell using capillary action. Commercial Grade N52 Neodymium block magnets were used to provide the external magnetic fields. Structures made from a diamagnetic material, copper, were used for control experiments, i.e. to study the uniform field case, as copper does not meaningfully alter the background field generated by the block magnets. All experiments were conducted at room temperature unless otherwise specified. For birefringent LCs imaged under crossed polarizers in POM, the field of view will be dark or bright based on the director orientation relative to the optical axis. 5CB has positive birefringence and so a molecule oriented along the optical axis will not modify the polarization of light (producing a dark field of view), while molecules perpendicular to the optical axis, or molecules in the plane of a sample cell, will.

For the experiments conducted here, the optical axis is parallel to 5CB mesogens that are anchored homeotropically at the glass surface. In the presence of an external magnetic field, regions of the NLC undergo a bend-type transition, where molecules now orient perpendicular to the optical axis. These regions appear bright provided the director is not parallel to either the polarizer or analyzer direction. The variation in transmitted light intensity as a function of

polarizer/analyzer orientation therefore conveys information regarding the orientation of the director. Images are taken at each field value after waiting several seconds. This procedure ensured sample equilibration.

FEM Of Spatially Varying Magnetic Fields

The magnetic field patterns that result from the cobalt structures are simulated using COMSOL Multiphysics®.

Numerical Relaxation of the LdG Free Energy

The simulated magnetic field data is imported into open-Qmin, an open-source code designed for lattice-discretized LdG modeling of LC systems.[21] Within open-Qmin, the geometry of the ferromagnetic structure and the homeotropic anchoring of 5CB at the structure surface are specified as boundary conditions, allowing for the simulation and visualization of the nematic LC director in the region around the ferromagnetic structure.

In open-Qmin, it is necessary to replace dimensionalized quantities with non-dimensionalized counterparts. All energy densities are scaled in units of the magnitude of the first LdG bulk free energy coefficient. The non-dimensionalization of the system is limited by the lattice spacing, which is approximately the size of one mesogen.

All simulations represented here are generated with dimensions of 240×240×28. This represents an NLC homeotropic slab cell that is approximately 1 μm in thickness and 10 μm by 10 μm wide. All parameters of this simulation are finely tuned for 5CB.[22, 23] Finally, we can use Jones calculus to model transmitted light intensity, where a Jones vector represents multicolored polarized light, and optical elements are represented by Jones matrices to simulate the pattern of the resultant LC director imaged under POM.[24]

RESULTS AND DISCUSSION

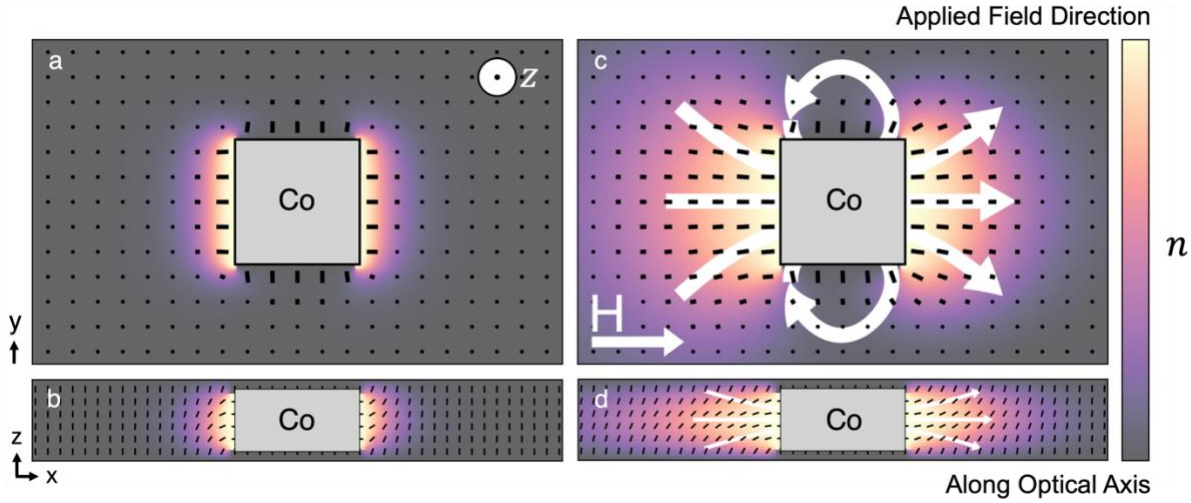

Figure 1. Spatially Modified Fréedericksz transition. The top row shows the top view, while the bottom row shows the side view of the LC cell. (a) and (b) Bright areas denote regions of strong alignment caused by director distortions in the homeotropic cell due to homeotropic anchoring at the Co sidewalls. (c) and (d) A background magnetic field is simulated using FEM and applied to the LC along the x-axis. The spatially modified field depicted with white arrows induces alignment of the nematogen. Concomitantly, the bright areas are enlarged relative to the field-free case (a).

We study small molecule LCs in the nematic phase confined in a homeotropic cell as they undergo a bend-type Fréedericksz transition. The critical field H_c required to induce this bend-type transition is derived from the distortion energy associated with nematogen bend and the magnetic contribution to the free energy. Here, the critical field H_c needed for a transition is

$$H_c = \frac{\pi}{d}\sqrt{\frac{K}{\mu_0 \Delta\chi}} \qquad (1)$$

where d is the spacing between the glass slides, K is the bend elastic constant, μ_0 is the vacuum magnetic permeability of free space, and $\Delta\chi$ is the anisotropic component of the magnetic susceptibility tensor of the LC.

Observations with POM confirm how the LC director responds to the custom-structured fields and thus transitions from the homeotropic to the planar configuration near critical field strengths. In this planar configuration, the local magnetic field direction spatially modifies the director and is encoded into the observed birefringence of the LC. In Figure 1, a simulated ferromagnetic cobalt microstructure (gray square) is placed in the bulk of a nematic homeotropic LC cell. The cell is treated such that the director lies along the optical axis, perpendicular to the glass slides. Bright areas amongst the homeotropic (dark gray) background indicate places where a component of the director lies along the axis of the magnetic field application.

In the zero-field case, the ferromagnet enforces anchoring in opposition with the homeotropic confinement of the slab cell that frustrates the LC, leading to a bright band around the object, as depicted in Figure 1a. The high permeability Co microstructure concentrates field lines as a field is externally applied, illustrated in Figure 1c. The external field is along the x-axis, so the field intensification is fore and aft of the structure, which results in the surface-induced distortion of the director extending significantly farther into the LC surrounding the Co along this direction. The bend transition, which is responsible for the distortion, exhibits a spatial dependence that reflects the field strength variation as a function of distance away from the Co – the field strength decays below the critical field required for the transition, and the LC is effectively undistorted beyond that point.

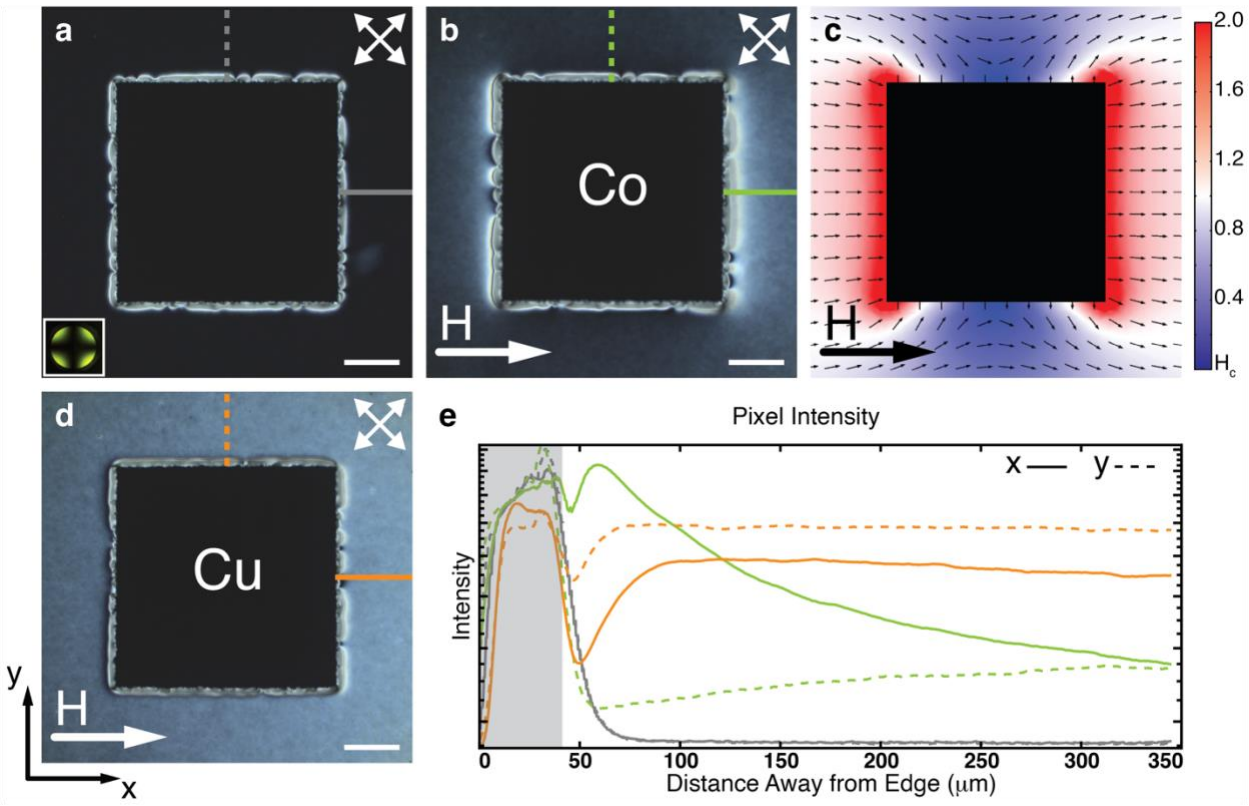

Figure 2. A Ferromagnetic Inclusion in a Homeotropic NLC Cell. (a) A POM image of the LC cell with a square-shaped cobalt structure in the absence of an external field. The inset on the bottom left is the conoscopic pattern which confirms that the LC is pointed along the optical axis. The orientations of the polarizer and analyzer are depicted in the top right. (b) A POM image of the LC cell in the presence of an external field. The white arrow indicates the applied field direction. (c) A FEM simulation of the intensity and direction of a magnetic field generated from the cobalt structure in the presence of a background magnetic field. (d) A POM image of the NLC cell with a copper structure in the presence of a field, as a control. (e) Pixel intensity is measured from the edge of the inclusions along and perpendicular to the field direction for (a), (c), and (d). The colors and styles of line represent the corresponding regions in each figure. The scale bar is 250 μm.

Experiments were conducted using POM to visualize the director configuration of the LC in the absence and presence of an external field. In the field-free case, the homeotropic LC cell appears dark due to the alignment of the LC along the optical axis, regardless of the orientation of the crossed polarizers. The dark field of view far from the Co structure reflects this scenario. However, a bright band occurs in close proximity to the Co surface (Figure 2a) due to the antagonistic anchoring constraints – the homeotropic cell enforces alignment along the optical axis, while the metal surface enforces anchoring perpendicular to its surface, and therefore orthogonal to the optical axis. The pixel intensity along the x- and y- directions are depicted as gray solid and dashed lines, respectively, in Figure 2e. Notably, the bright band is about 50 μm wide, and the intensity is near-zero beyond 50 μm.

Figure 2b, shows the system in the presence of the external field. The cobalt distorts the field strength and direction due to its high permeability relative to the surrounding medium, and the LC director varies accordingly. During the reorientation of the director, we do not observe any newly formed defects. The crossed polarizers are placed such that a director with a component along the x-axis will appear bright (i.e. at 45° relative to the field). The director alignment resulting from the field is captured by the corresponding pixel intensity, mapped along a green solid line in Figure 2b. The intensity profile has a peak beyond 50 μm and gradually falls off. Simultaneously, other regions in the bulk of the sample, where the field is below the value, retain their homeotropic alignment and appear dark. Figure 2b illustrates that the areas above and below the cobalt structure in the image remain dark due to the suppression of the background field. Away from the object, the field suppression is negligible, and the measured intensity along the horizontal (solid) and vertical (dashed) lines shrinks and grows, respectively, as apparent in Figure 2e. Both measured

intensities from the object converge to the same value corresponding to the bulk LC responding to the applied background field.

The absence of the bend transition above and below the Co in the image, and the enhanced penetration of director distortion along the x-axis are consistent with the expected suppression and intensification of the field in these regions, respectively, as reflected in field simulations rendered for this geometry (Figure 2c). The red and blue regions denote where the field has been respectively enhanced or suppressed relative to the background applied field, with field strength displayed in units of critical field strength, H_c. Figure 2d features a control experiment using a copper structure that does not distort the applied field significantly enough to promote director distortions. As the external field strength increases, birefringence uniformly intensifies across the NLC cell in both the x- and y-directions as seen from the corresponding pixel traces in Figure 2e. The profiles do not exhibit spatial variation.

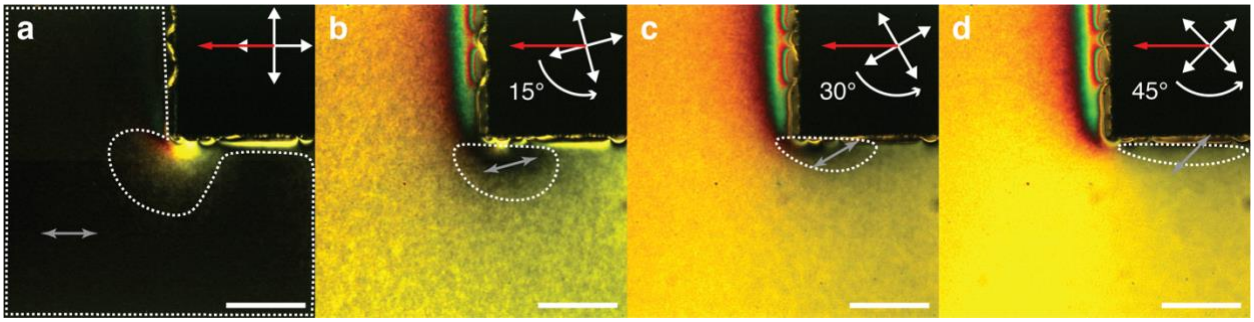

Figure 3. Director Orientation Varying Along Magnetic Field. Polarizers are rotated (a) 0° (b) 15° (c) 30° (d) 45° counterclockwise, from an initial position in which one polarizer is parallel to the field. A shift in the dark and bright regions illustrates the variation in the director orientation. The director in the white dashed regions is oriented as illustrated by the gray double arrows. The direction of magnetic field is left-right, indicated by the red arrows. The scale bar is 100 μm.

Further studies of the spatially distorted director configuration are conducted via rotation of the crossed polarizers, with results shown in Figure 3. The orientation of molecules that lie in the plane of the page can be determined, and we confirm that the transitioned director lies along the magnetic field lines generated by the ferromagnetic object shown in Figure 2c. Nematogens that lie along the polarizer or analyzer axis will appear dark. In contrast, regions where nematogens lie off the polarizer and analyzer axis will have a higher transmitted light intensity due to the birefringence of the nematogen. As the polarizer and analyzer axis is rotated, a director orientation can be prescribed to areas where the sample remains dark, matching the polarizer's or analyzer's orientation.

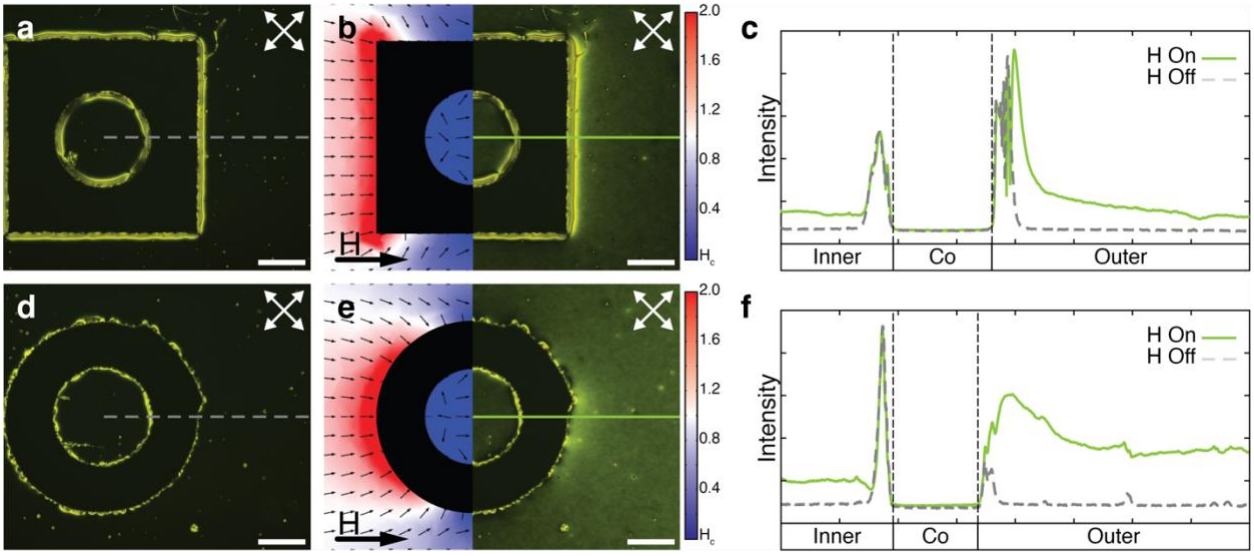

Figure 4. Vanishing stimuli using Ferromagnets in Homeotropic NLC Cells. (a) POM images under crossed polarizers of LC in and around a hollow cobalt square in the absence of the applied field. (b) Simulated magnetic field in and around the hollow square (left) and the POM image (right) of the system in the presence of an applied field oriented 45° relative to the crossed polarizers. The white crossed double-arrows indicate the orientations of the polarizer and analyzer. The thick black arrow indicates the applied field direction. The scale bar is 250 μm. (c) Pixel intensity profiles along the corresponding-colored lines for the field-free and applied field cases are shown. (d)-(f) Corresponding data for hollow ring structure. The scale bar is 250 μm.

Figure 4 demonstrates the LC patterns generated from hollow square and ring plate geometries. Based on field simulations in Figure 4b and e, the value of the applied background field can be tuned such that the field strength inside the plate hollow is significantly lower than the critical field, H_c, required to induce a director response. We show in Figure 4b and e that regions in the center area remain relatively dark at background field strengths $H > H_c$ that are expected to induce a director transition. The pixel intensity profiles, shown in Figure 4c and f, indicate that the LC outside the hollow regions has undergone a transition while the material inside the hollows is

relatively unperturbed by the field – the corresponding light intensity is lower than that from regions outside the hollow. This demonstrates the ability to effectively suppress the effect of an applied magnetic field on a LC medium through the use of appropriately designed magnetic constructs.

The cobalt plates used so far represent only some of the various cobalt structures investigated using COMSOL Multiphysics®, free-energy simulations, and POM observations. Figure S5 showcases the LC director obtained from different cobalt structures, such as the U-shaped structure or square arrays. Each cobalt arrangement leads to distinct deformation hotspots dependent on the anchoring effects and the spatially varying fields produced. This approach allows flexibility in programming diverse customizable LC director patterns. The resultant LC director configuration can be tweaked to design bespoke responsive materials. We imagine interference-like patterns of static magnetic fields could be imprinted onto the NLC.[25] Further, in LC elastomers, controlling the LC using customized fields could be used to induce complex shape-change actuation.[26]

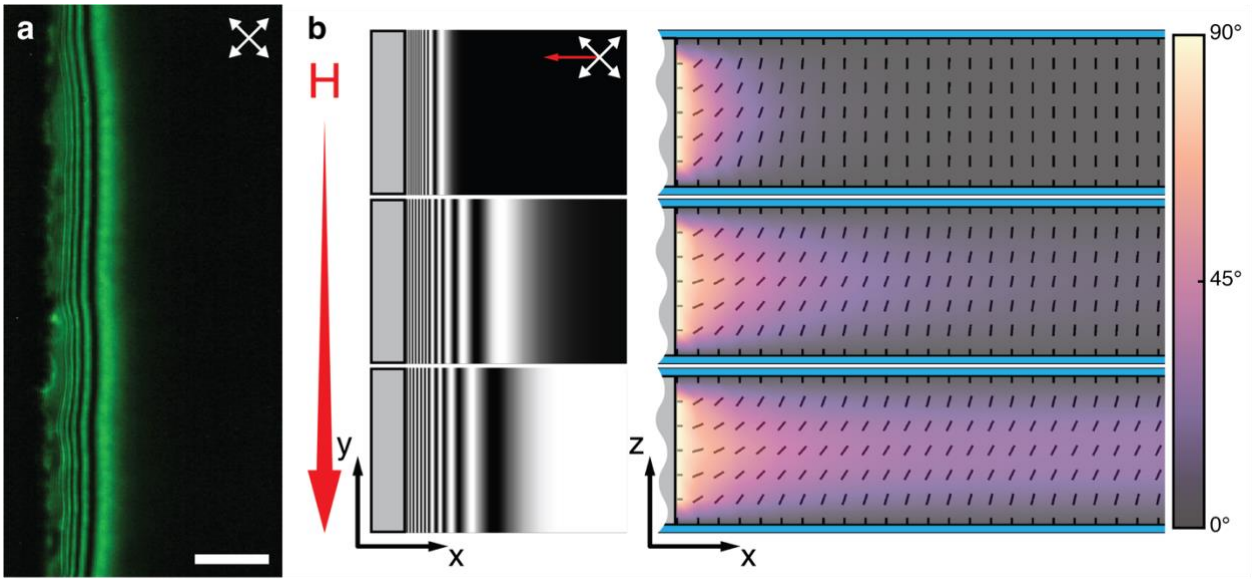

Figure 5. Propagation of Optical Fringes Near a Ferromagnet. (a) A POM image of fringes near the edge of a cobalt structure in the absence of an external field. Green light is used. (b) Simulated POM images of fringes (Left) as an external field is applied—corresponding director configurations of xz-plane (Right). The color bar indicates the angle between the director and the optical axis (z-axis). A slice of the simulated director near the ferromagnetic wall is plotted, where the black line segments indicate the LC nematic director orientation. The background color depicts the director's orientation from 0° to 90° with respect to the optical axis. The propagated light intensity is calculated to obtain the optical pattern from these 2D director plots, assuming uniformity in the third dimension (along the y-axis). The scale bar is 50 μm.

Distortions in the director were studied under POM using single-color illumination produced by an optical filter. As shown in Figure 5a, dark and bright fringes emanate outward from the edges of the ferromagnetic structure in the field-free case. The spatial variation in the orientation of the dielectric tensor of the LC generates a quasi-sinusoidal spatial variation in the intensity of light transmitted through the sample. This effect is due to competition in the constraints acting on the director from the cobalt edge to the cell substrate, as seen previously in related systems.[27-29] The

homeotropic constraints from both the cell and cobalt surfaces force a bend in the director. The continuum theory of the LC described the bend response of the director subject to antagonistic homeotropic anchoring conditions. In the absence of an external field in the two-dimensional, one elastic constant approximation, the analytical solution of director orientation is

$$\theta(x,z) = \sum_{\substack{n=1 \\ n\ is\ odd}}^{\infty} \frac{2}{n} e^{-\frac{n\pi}{d}x} \sin\left(\frac{n\pi}{d}z\right), n \in \mathbb{Z}^{+} \quad (2)$$

where θ is the angle between director and optical axis (z-axis) and d is the thickness of NLC cell (details in Supporting Information). The intensity profile resulting from this continuous director variation is sinusoidally damped, and alternating bright and dark fringes concentrated near the source of the distortion are therefore anticipated. This solution predicts the location of the outermost bright fringe at $x_\xi \approx 0.64d$. This effectively represents the penetration length or the distance into the LC over which the director is distorted. The fringes are an explicit manifestation of the penetration of director distortion produced by an inclusion (the cobalt surface) into an LC medium, and their locations encode information about the medium's susceptibility to distortion. The experimentally measured penetration length is smaller than the theoretical prediction, with $x_\xi \approx 0.58d$.

The disparity between the theoretical and experimentally observed widths could be due to the assumption of perfect anchoring conditions at the edge of the structure in the simulation. The actual surface is rough, and the surface normal is therefore not uniform. Any departure from uniform homeotropic anchoring on the cobalt surface would result in a smaller penetration length as less director distortion is then required to accommodate the antagonistic anchoring at the glass surface.

We surmise therefore that surface roughness, or any otherwise non-uniform homeotropic anchoring leads to a smaller x_ξ.

In the presence of a field, the region over which the bend occurs, and, consequently, over which the fringes are observed, increases in extent. Numerical solutions for the continuous deformation of the director as the external field is increased are obtained via free energy minimization under a uniform field approximation. The corresponding director configuration and resulting fringes are visualized in Figure 5b. As the field increases, the compact fringes spread along the field direction, away from the cobalt surface. This smearing is due to a larger region of LC molecules reorienting toward the field direction.

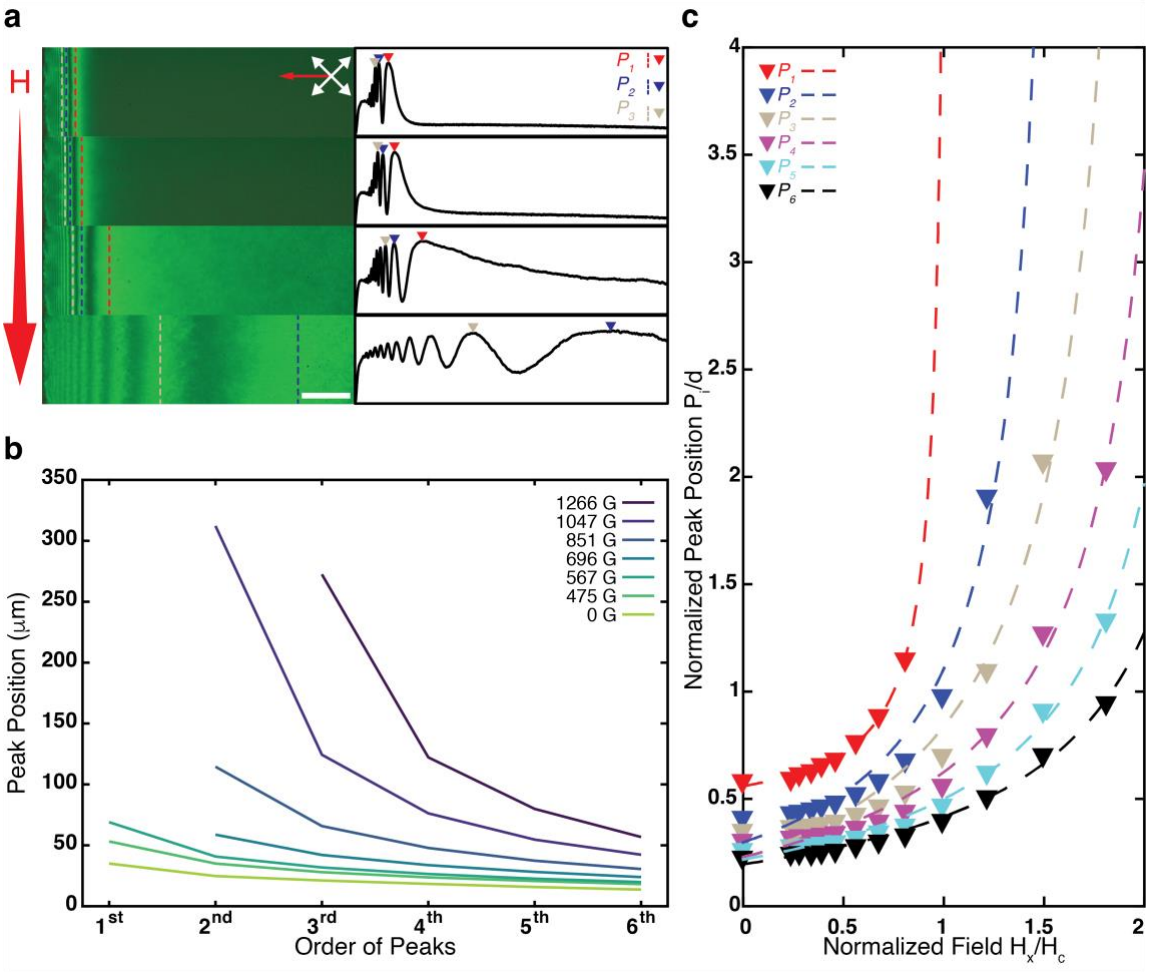

Figure 6. Fringes Under Increasing Field Strength. (a) The single-color-illumination POM images of the NLC regions alongside the cobalt structure as the external field increases alongside the corresponding intensity profiles of the observed fringes. The red, blue, and gray triangles and dashed lines mark the position of the first, second, and third peaks (P_1, P_2, and P_3) of the measured fringe intensities, respectively. The field is applied in the plane of the NLC cell at an angle of 45° to the crossed polarizers. The scale bar is 50 μm. The cell thickness is 60 μm. (b) The position of each peak order at different applied fields is plotted. (c) The position of each peak order changes with increasing applied field. The dashed lines representing peak position are fit to the applied field strength using Equation 3.

We investigated the motion of fringes away from the cobalt surface in response to increasing applied field strengths. Results are shown in Figure 6. Consistent with simulations, the fringes move laterally away from the ferromagnetic structure as the field strength increases. Figure 6a tracks bright peak positions at different applied field strengths. Based on the positions of each peak, a field strength chart could be generated, and representative data for such a plot can be utilized in Figure 6b. This chart allows us to estimate the magnetic field strength applied to a structure based on corresponding observable peak positions, demonstrating the potential usage of this phenomenon for field sensing applications.

Moreover, it is noticeable that each fringe peak not only moves away from the wall with increasing field but also becomes broader, as shown in Figure 6a. For example, tracking the first peak P_1 in Figure 6a, marked by a red inverted triangle, we find it evolves from a narrow peak to a broad one and at large enough field is smoothed out entirely. We call this phenomenon "fringe escape" and define the field strength causing the fringe escaping, "escape field" $H_{E,i}$, where subscript i indicating the order of peak, such as 1st, 2nd or etc. Figure 6c illustrates the peak position of each order of peaks as a function of field strength. Each curve diverges as it approaches a critical field, which represents the escape field. The data are fit using the following expression,

$$\widetilde{\mathrm{P}}_i = \frac{\alpha}{\widetilde{H} - \widetilde{H}_{E,i}} + \beta \qquad (3)$$

where $\widetilde{\mathrm{P}}_i$ is the peak position of i$^{\text{th}}$ peak normalized by the cell thickness, and α and β are the fitting parameters, and $\widetilde{H}_{E,i}$ is the escape field normalized by the critical field for the bend transition. We conclude that higher order peaks have higher escape fields based on the result shown in Figure 6c. Our results show that the escape field for the first peak coincides with the critical field for the

Fréedericksz transition, i.e. $\widetilde{H}_{E,1} \approx 1$. This is consistent with the notion that the escape of the primary bright fringe represents the first far-field penetration of director distortion into the LC medium.

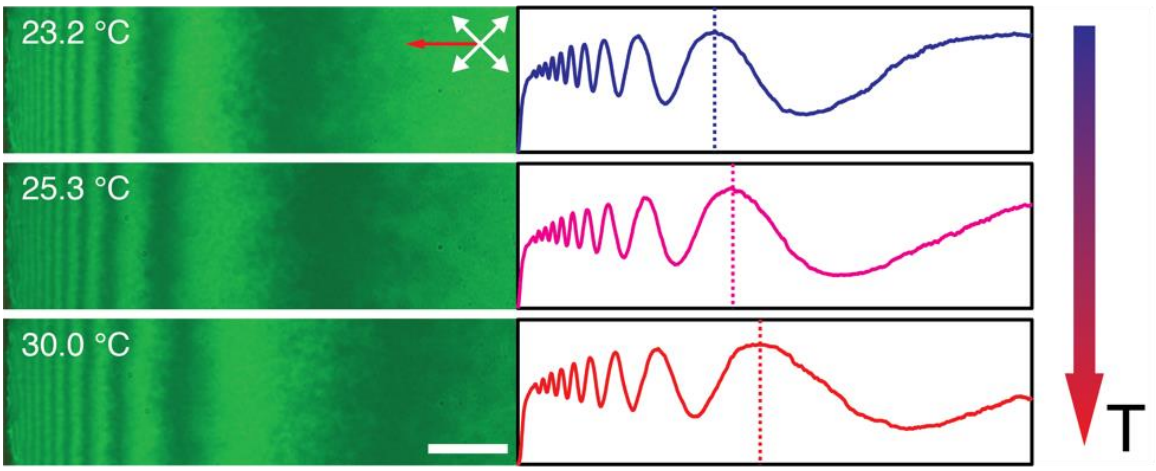

Figure 7. Fringes at Different Temperatures. POM images of fringes in the LC cell adjacent to a cobalt structure. An external field is applied at different temperatures, and corresponding intensity profiles are measured. The field is applied in-plane with respect to LC cell with an angle of 45° to the polarizer/analyzer. The scale bar is 50 μm.

The response of the LC to the applied magnetic field depends intrinsically on the magnitude of the bend elasticity relative to the anisotropy of the LC magnetic susceptibility, $K/\Delta\chi$. Both K and $\Delta\chi$ are temperature dependent quantities that vanish above the nematic-isotropic transition temperature. We investigate the system's temperature-dependent response in the nematic phase. The applied field was held constant while the NLC cell was heated from 23.2 to 30 °C. These temperatures are well-removed from the nematic-isotropic transition temperature of 35.5 °C. As shown in Figure 7, the fringe spacing increases with temperature, highlighting greater penetration of the director distortion into the LC. Our results indicate that the ratio between bend elastic constant and anisotropy of magnetic susceptibility decreases with temperature. This is consistent with reported temperature dependent property data for 5CB.[30] The temperature-dependent fringe motion provides a means of characterizing the temperature-dependence of $K/\Delta\chi$.

CONCLUSION

This study highlights the intricate interplay between magnetic structures and a surrounding LC director. We investigated the impact of cobalt structures on local magnetic fields, revealing complex distortions in field direction and strength. These distortions lead to spatial variations in the field strength and associated responses of the LC. The presence of antagonistic anchoring conditions gives rise to optical fringes that encode the susceptibility of the LC to the penetration of director distortion. A field normally applied to the distortion-inducing surface increases fringe penetration and fringe migration into the LC as the director distortion spreads into the far field of the medium. Fringe escape occurs at particular values of the applied field, with the escape of the primary fringe coincident with the critical field for the Fréedericksz transition. Fringe motion is also observed as a function of temperature at fixed applied fields. It reflects temperature dependence in the ratio of the bend elastic constant to the magnetic susceptibility anisotropy. The ability to both significantly suppress and enhance the external field in appropriately constructed geometries suggests that deliberately designed magnetic structures can create complex director configurations in LC materials, potentially in support of new liquid crystal technologies. An interesting “inverse-design” challenge is associated with deducing the arrangement of structures that will produce a magnetic field to yield a particular desired director configuration. Our investigation of the fringe formation and spacing in the LC cell under varying external field strengths unveiled a remarkable sensitivity that could be harnessed for field sensing applications. Correspondingly, temperature-dependent fringe motion at fixed fields provides a simple means of characterizing temperature-dependent LC properties.

ASSOCIATED CONTENT

Additional experimental details, materials, and methods, including photographs of experimental setup. A description of two formulations to simulate the LC director and corresponding intensity profiles including a GitHub. Field and LC director simulations obtained from different cobalt structures. Additional data for LC fringe response to increased field strength. (docx)

AUTHOR INFORMATION

Corresponding Author

* Corresponding author: E-mail address: cosuji@seas.upenn.edu

Author Contributions

The manuscript was written through contributions of all authors. All authors have given approval to the final version of the manuscript. ‡These authors contributed equally.

Funding Sources

This work was supported by NSF through DMR- 2223705 and DGE- 2152205, and in part by a Simons Investigator grant from the Simons Foundation to R.D.K.

ACKNOWLEDGMENT

We want to express our gratitude to Dan Beller and Daniel Sussman for their invaluable contributions to this work through the development of openQmin. Their efforts in implementing the capability to handle spatially varying magnetic field files have been instrumental in this study.

REFERENCES

(1) Lavrentovich, O. D. Liquid Crystals, Photonic Crystals, Metamaterials, and Transformation Optics. *Proceedings of the National Academy of Sciences* **2011**, *108* (13), 5143-5144. DOI: doi:10.1073/pnas.1102130108.

(2) Xu, J.; Yang, R.; Fan, Y.; Fu, Q.; Zhang, F. A Review of Tunable Electromagnetic Metamaterials with Anisotropic Liquid Crystals. *Frontiers in Physics* **2021**, *9*, 1-14, Review. DOI: 10.3389/fphy.2021.633104.

(3) Xia, Y.; Cedillo-Servin, G.; Kamien, R. D.; Yang, S. Guided Folding of Nematic Liquid Crystal Elastomer Sheets into 3d Via Patterned 1d Microchannels. *Adv Mater* **2016**, *28* (43), 9637-9643. DOI: 10.1002/adma.201603751 From NLM.

(4) Tran, L.; Lavrentovich, M. O.; Beller, D. A.; Li, N.; Stebe, K. J.; Kamien, R. D. Lassoing Saddle Splay and the Geometrical Control of Topological Defects. *Proceedings of the National Academy of Sciences* **2016**, *113* (26), 7106-7111. DOI: doi:10.1073/pnas.1602703113.

(5) Kim, D. S.; Čopar, S.; Tkalec, U.; Yoon, D. K. Mosaics of Topological Defects in Micropatterned Liquid Crystal Textures. *Sci Adv* **2018**, *4* (11), eaau8064. DOI: 10.1126/sciadv.aau8064 From NLM.

(6) Guin, T.; Settle, M. J.; Kowalski, B. A.; Auguste, A. D.; Beblo, R. V.; Reich, G. W.; White, T. J. Layered Liquid Crystal Elastomer Actuators. *Nature Communications* **2018**, *9* (1), 2531. DOI: 10.1038/s41467-018-04911-4.

(7) Wang, Y.; An, J.; Kim, H.; Jeong, S.; Kim, H.; Park, J.; Ko, S.; Son, J.; Lee, H. Printing Mosaics of Magnetically Programmed Liquid Crystal Directors for Reversibly Morphing Soft Matter. **2024**, 1-39. DOI: 10.48550/arxiv.2401.06590.

(8) Ware, T. H.; McConney, M. E.; Wie, J. J.; Tondiglia, V. P.; White, T. J. Voxelated Liquid Crystal Elastomers. *Science* **2015**, *347* (6225), 982-984. DOI: doi:10.1126/science.1261019.

(9) Kim, Y.; Yuk, H.; Zhao, R.; Chester, S. A.; Zhao, X. Printing Ferromagnetic Domains for Untethered Fast-Transforming Soft Materials. *Nature* **2018**, *558* (7709), 274-279. DOI: 10.1038/s41586-018-0185-0.

(10) Lesiuk, A. I.; Ledney, M. F.; Reshetnyak, V. Y. Light-Induced Fredericks Transition in the Nematic Liquid Crystal Cell with Plasmonic Nanoparticles at a Cell Bounding Substrate. *Phys Rev E* **2022**, *106* (2), 024706. DOI: 10.1103/PhysRevE.106.024706.

(11) Yang, D.-K.; Wu, S.-T. *Fundamentals of Liquid Crystal Devices*; John Wiley & Sons, Incorporated, 2014.

(12) Ettinger, S.; Slaughter, C. G.; Parra, S. H.; Kikkawa, J. M.; Collings, P. J.; Yodh, A. G. Magnetic-Field-Driven Director Configuration Transitions in Radial Nematic Liquid Crystal Droplets. *Phys Rev E* **2023**, *108* (2). DOI: ARTN 02470410.1103/PhysRevE.108.024704.

(13) Gopinadhan, M.; Choo, Y.; Kawabata, K.; Kaufman, G.; Feng, X.; Di, X.; Rokhlenko, Y.; Mahajan, L. H.; Ndaya, D.; Kasi, R. M.; Osuji, C. O. Controlling Orientational Order in Block Copolymers Using Low-Intensity Magnetic Fields. *Proceedings of the National Academy of Sciences* **2017**, *114* (45), E9437-E9444. DOI: doi:10.1073/pnas.1712631114.

(14) Rokhlenko, Y.; Gopinadhan, M.; Osuji, C. O.; Zhang, K.; O'Hern, C. S.; Larson, S. R.; Gopalan, P.; Majewski, P. W.; Yager, K. G. Magnetic Alignment of Block Copolymer Microdomains by Intrinsic Chain Anisotropy. *Physical Review Letters* **2015**, *115* (25), 258302. DOI: 10.1103/PhysRevLett.115.258302.

(15) Zhang, J.; Guo, Y.; Hu, W.; Soon, R. H.; Davidson, Z. S.; Sitti, M. Liquid Crystal Elastomer-Based Magnetic Composite Films for Reconfigurable Shape-Morphing Soft Miniature Machines. *Advanced Materials* **2021**, *33* (8), 2006191. DOI: https://doi.org/10.1002/adma.202006191.

(16) Kim, D.; Ndaya, D.; Bosire, R.; Masese, F. K.; Li, W.; Thompson, S. M.; Kagan, C. R.; Murray, C. B.; Kasi, R. M.; Osuji, C. O. Dynamic Magnetic Field Alignment and Polarized Emission of Semiconductor Nanoplatelets in a Liquid Crystal Polymer. *Nature Communications* **2022**, *13* (1), 2507. DOI: 10.1038/s41467-022-30200-2.

(17) Li, Z.; Wang, J.; Zou, J.; Li, S.; Zhen, X.; Shen, Z.; Li, B.; Zhang, X.; Nan, C.-W. Magnetic-Assisted Alignment of Nanofibers in a Polymer Nanocomposite for High-Temperature Capacitive Energy Storage Applications. *Materials Horizons* **2024**, *11* (18), 4472-4481, 10.1039/D4MH00493K. DOI: 10.1039/D4MH00493K.

(18) Chandrasekhar, S. *Liquid Crystals*; Cambridge University Press, 1992. DOI: DOI: 10.1017/CBO9780511622496.

(19) Dierking, I. *Textures of Liquid Crystals*; Wiley-VCH, 2003.

(20) Nogami, T.; Nakada, T.; Sakai, R.; Hosoya, T. Process for Forming a Liquid Crystal Vertical Alignment Film. United States 5766673, 1998.

(21) Sussman, D. M.; Beller, D. A. Fast, Scalable, and Interactive Software for Landau-De Gennes Numerical Modeling of Nematic Topological Defects. *Frontiers in Physics* **2019**, *7*, 1-15, Original Research. DOI: 10.3389/fphy.2019.00204.

(22) Gharbi, M. A.; Seč, D.; Lopez-Leon, T.; Nobili, M.; Ravnik, M.; Žumer, S.; Blanc, C. Microparticles Confined to a Nematic Liquid Crystal Shell. *Soft Matter* **2013**, *9* (29), 6911-6920, 10.1039/C3SM00126A. DOI: 10.1039/C3SM00126A.

(23) Kosa, T.; Palffy-muhoray, P. Magnetic Field Induced Deformations in Nematic Liquid Crystals. *Liquid Crystals Today* **1996**, *6* (1), 7-8. DOI: 10.1080/13583149608047632.

(24) Lien, A. A Detailed Derivation of Extended Jones Matrix Representation for Twisted Nematic Liquid Crystal Displays. *Liquid Crystals* **1997**, *22* (2), 171-175. DOI: 10.1080/026782997209531.

(25) Yang, Z.; Wei, J.; Giżynski, K.; Song, M.-G.; Grzybowski, B. A. Interference-Like Patterns of Static Magnetic Fields Imprinted into Polymer/Nanoparticle Composites. *Nature Communications* **2017**, *8* (1), 1564. DOI: 10.1038/s41467-017-01861-1.

(26) Visschers, F. L. L.; Hendrikx, M.; Zhan, Y.; Liu, D. Liquid Crystal Polymers with Motile Surfaces. *Soft matter* **2018**, *14* (24), 4898-4912. DOI: 10.1039/c8sm00524a.

(27) Yesil, F.; Suwa, M.; Tsukahara, S. Anchoring Energy Measurements at the Aqueous Phase/Liquid Crystal Interface with Cationic Surfactants Using Magnetic Fréedericksz Transition. *Langmuir* **2018**, *34* (1), 81-87. DOI: 10.1021/acs.langmuir.7b03005.

(28) Kędzierski, J.; Raszewski, Z.; Kojdecki, M.; Kruszelnicki-Nowinowski, E.; Perkowski, P.; Piecek, W.; Miszczyk, E.; Zieliński, J.; Morawiak, P.; Ogrodnik, K. Determination of Ordinary

and Extraordinary Refractive Indices of Nematic Liquid Crystals by Using Wedge Cells. *Opto-Electronics Review* **2010**, *18* (2), 214-218. DOI: doi:10.2478/s11772-010-0009-8 (acccessed 2024-11-13).

(29) Guo, T.; Zheng, X.; Palffy-Muhoray, P. The Freedericksz Transition in a Spatially Varying Magnetic Field. *Crystals (Basel)* **2021**, *11* (5), 541. DOI: 10.3390/cryst11050541.

(30) Bradshaw, M. J.; Raynes, E. P.; Bunning, J. D.; Faber, T. E. The Frank Constants of Some Nematic Liquid Crystals. *Journal de Physique* **1985**, *46* (9), 1513-1520. DOI: 10.1051/jphys:019850046090151300 Ajp.

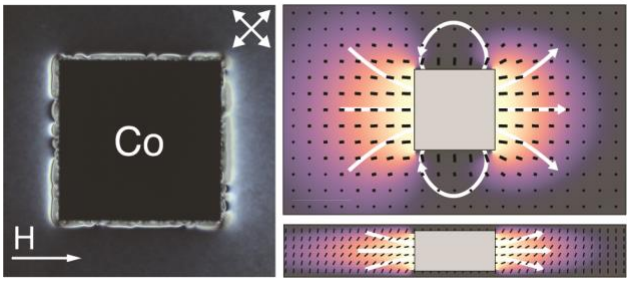

For Table of Contents Only